Far-Infrared Optical Conductivity Gap in Superconducting MgB_2 Films

Robert A. Kaindl, Marc A. Carnahan, Joseph Orenstein, and Daniel S. Chemla
Department of Physics, University of California at Berkeley, and Materials Sciences Division, E. O. Lawrence Berkeley National Laboratory, Berkeley, California 94720

Hans M. Christen, Hong-Ying Zhai, Mariappan Paranthaman, and Doug H. Lowndes
Solid State Division, Oak Ridge National Laboratory, Oak Ridge, Tennessee 37931-6056
(Received 20 June 2001; published 28 December 2001)

We report the first study of the optical conductivity of MgB_2 covering the range of its lowest-energy superconducting gap. Terahertz time-domain spectroscopy is utilized to determine the complex, frequency-dependent conductivity $\sigma(\omega)$ of thin films. The imaginary part reveals an inductive response due to the emergence of the superconducting condensate. The real part exhibits a strong depletion of oscillator strength near 5 meV resulting from the opening of a superconducting energy gap. The gap ratio of $2\Delta_0/k_BT_C \approx 1.9$ is well below the weak-coupling value, pointing to complex behavior in this novel superconductor.

DOI: 10.1103/PhysRevLett.88.027003 PACS numbers: 74.70.Ad, 42.62.Fi, 78.30.Er

The recent discovery of superconductivity in MgB_2 at 39 K has spawned intense research efforts, yet the nature of its remarkably high transition temperature remains to be understood [1]. While the isotope effect points to phonon-mediated mechanisms [2], its anomalous magnitude [3] and distinctly different values found for the superconducting energy gap $2\Delta_0$ [4–12] seem puzzling. First-principles band-structure calculations indicate that the dominant hole carriers in Boron p orbitals are split into two distinct sets of bands with quasi-2D and 3D character [13]. Among phonon-mediated mechanisms which attempt to explain the high T_C are anisotropic two-gap scenarios where the quasi-2D holes couple preferentially [14], strong coupling Eliashberg calculations including low- and high-energy modes [15], or nonadiabatic superconductivity [16].

The prospect of unconventional coupling or an anisotropic order parameter motivates experiments which probe the density of states, governed foremost by the superconducting energy gap. Different heat capacity [4,5] and Raman [6,7] studies of bulk material each yielded important but contradictory information about the gap excitations. Moreover, surface probes such as tunneling and photoemission found very different values for the gap $2\Delta_0$ ranging from 4–14 meV in polycrystalline MgB_2 [8–12]. Recent point contact experiments found regions where two distinct conductance peaks of different magnitude appear ($2\Delta_0 = 6$ and 14 meV) [11,12]. Possible reasons for this large variation could include proximity or compositional effects that remain hidden in the bulk T_C [9,10]. The most fascinating prospect is a possible coexistence of two superconducting gaps following recent theoretical predictions [14].

Optical probes offer important advantages since they penetrate appreciably inside the bulk, where they probe the spectrum of low-energy excitations including the superconducting energy gap [17]. In addition, the complex conductivity represents a simultaneous, contactless measure of the condensate within the sampled volume. In MgB_2, a first measurement of far-infrared reflectivity in granular samples showed an increase below $\hbar\omega \lesssim 9$ meV [18], while the transmission through films also increases in that range [19]. While this could stem from a gap in the real part of the optical conductivity, the necessary Kramers-Kronig transformations mandate measurements over a much broader spectral range and with high precision. Thus, direct measurements of the conductivity are crucial. First results at low photon energies (0.5–3.7 meV), however, found no characteristic signature of a Bardeen-Cooper-Schrieffer (BCS) gap in that range [20].

In this Letter, we present the first measurement of the far-infrared conductivity of MgB_2 in a broad frequency range that spans excitations across its lowest-energy superconducting gap. The complex conductivity $\sigma(\omega)$, measured in transmission, reveals information about these fundamental excitations. Below T_C the real part of the conductivity is dominated by the depletion of oscillator strength due to the opening of a superconducting gap, while the imaginary part displays the inductive response of the condensate. The normal state scattering rate exceeds the gap energy. We find a gap size of $2\Delta_0 \approx 5$ meV, which is only half the value expected for an isotropic BCS gap.

Highly crystalline, superconducting films of MgB_2 were grown in a two-step process. Deposition of B precursor films via electron-beam evaporation was followed by *ex situ* postannealing at 890 °C in the presence of bulk MgB_2 and Mg vapor [21]. For the optical measurements, we investigate films of 100 and 200 nm thickness on Al_2O_3 substrates, with corresponding T_C's (zero resistance) of 30.5 and 34 K [inset, Fig. 1(a)] [22]. Scanning electron microscopy shows dense films with surface roughness

 © 2002 The American Physical Society

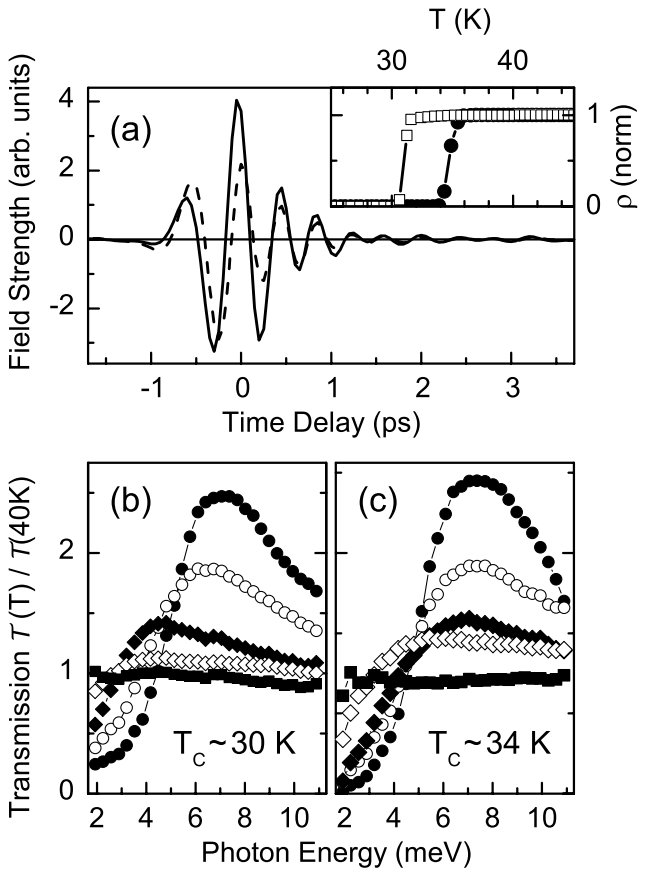

FIG. 1. (a) Electric field transients transmitted through the 100 nm MgB_2 film at $T = 6$ K (solid line) and 40 K (dashed line). Inset: resistance of the 200 nm (dots) and 100 nm (open squares) film corresponding to $\rho(40\ \mathrm{K}) \approx 10$ and 100 $\mu\Omega$ cm, respectively. (b) Transmission $\mathcal{T}$ normalized to $\mathcal{T}(40\ \mathrm{K})$ as obtained from the transients for the 100-nm-thick film at $T =$ 6 K (dots), 20 K (open circles), 27 K (solid diamonds), 30 K (open diamonds), and 33 K (solid squares). (c) Results for the 200-nm-thick film at $T = 6$ K (dots), 20 K (open circles), 25 K (solid diamonds), 30 K (open diamonds), and 36 K (solid squares).

below 5 nm for the 100 nm film, and a grainlike morphology similar to Ref. [21] was found for the thicker film.

In our experiment terahertz time-domain spectroscopy is used to determine the *complex* transmission function in the spectral range of interest without the need for Kramers-Kronig transformation [23]. Femtosecond near-infrared pulses from a 250 kHz Ti:sapphire amplifier are focused onto 0.5-mm-thick $\langle 110 \rangle$ oriented ZnTe crystals to generate and detect far-infrared pulses. This broadband far-infrared radiation (2–11 meV photon energy) is transmitted through the MgB_2 film mounted at normal incidence in a continuous-flow He cryostat equipped with Mylar windows.

Figure 1(a) shows the measured time-dependent electric field $E(t)$ of far-infrared pulses transmitted through the MgB_2 film in the superconducting and normal states. Below T_C (solid line), the pulse exhibits an increase of its field amplitude along with an apparent phase shift. This reshaping is linked to the changes of the frequency-dependent conductivity in the superconducting state. Fourier transformation of the incident and transmitted fields, $E_i(t)$ and $E_t(t)$, yields spectral information via the complex transmission coefficient $t(\omega) = E_t(\omega)/E_i(\omega)$. The power transmission spectrum $\mathcal{T}(\omega) = |t(\omega)|^2$, normalized to its 40 K normal state value, is shown in Figs. 1(b) and 1(c) for the 100- and 200-nm-thick samples, respectively. Above T_C, the transmission remains unchanged [solid squares, Figs. 1(b) and 1(c)], but below T_C a transmission increase is observed in a broad spectral range. Its peak shifts to higher photon energies with decreasing temperature. At the lowest temperature (solid dots), a more than twofold increase is found for photon energies around 7 meV, concurrent with a strong decrease below 4.5 meV. The response of the two samples is similar and, most notably, the spectral features occur at an identical position.

A more detailed understanding can be derived from the frequency-dependent complex conductivity $\sigma(\omega) = \sigma_1(\omega) + i\sigma_2(\omega)$ of the film, which is obtained from the measured transmission function at normal incidence in the thin-film limit via $\sigma = [(1 + n_s)t_f/t_s - n_s - 1]/Z_0 d$ [23]. Here, Z_0 is the impedance of free space, d is the film thickness, n_s is the substrate refractive index, and t_f and t_s are the complex transmission coefficients of film + substrate, and substrate, respectively. The thin-film approximation ($n_{\mathrm{film}}\omega d/c \ll 1$) is fulfilled well for the 100 nm film [transmission coefficient $|t(\omega)| \approx 0.1$], but the 200 nm film is optically too thick and thus was not evaluated quantitatively in this manner.

Absolute values of the normal state conductivity are shown in the inset of Fig. 2 for both the real part (circles) and imaginary part (squares). In the simplest case, the results can be compared to a single-component Drude conductivity $\sigma(\omega) = \epsilon_0 \omega_{\mathrm{pl}}^2/(\tau^{-1} - i\omega)$. A least-squares fit to the real and imaginary parts (solid lines) yields a plasma frequency $\omega_{\mathrm{pl}} = 12\,000 \pm 1500\ \mathrm{cm}^{-1}$ (1.5 eV) and scattering rate $\tau^{-1} = 300 \pm 70\ \mathrm{cm}^{-1}$ (37 meV). Even for a strong coupling gap of $\approx$10 meV this corresponds to the so-called dirty limit $\hbar/\tau \gg 2\Delta$ in which absorption should set in for photon energies exceeding the gap energy 2Δ since elastic scattering enables momentum conservation to the final state.

The ratio of the experimentally determined real part of the conductivity $\sigma_1(\omega)$ to its normal state value is plotted in Fig. 2 for different temperatures. As expected, the changes are small above T_C (diamonds), yielding a ratio close to 1. As the temperature falls below T_C a strong depletion of σ_1 is observed: the conductivity is smallest around 4.5 meV and then increases monotonically at higher photon energies. The steepest slope is obtained at the lowest temperature (6 K, dots) revealing a strong absorption onset near $\approx$5 meV. Results for the corresponding imaginary part of the conductivity $\sigma_2(\omega)$

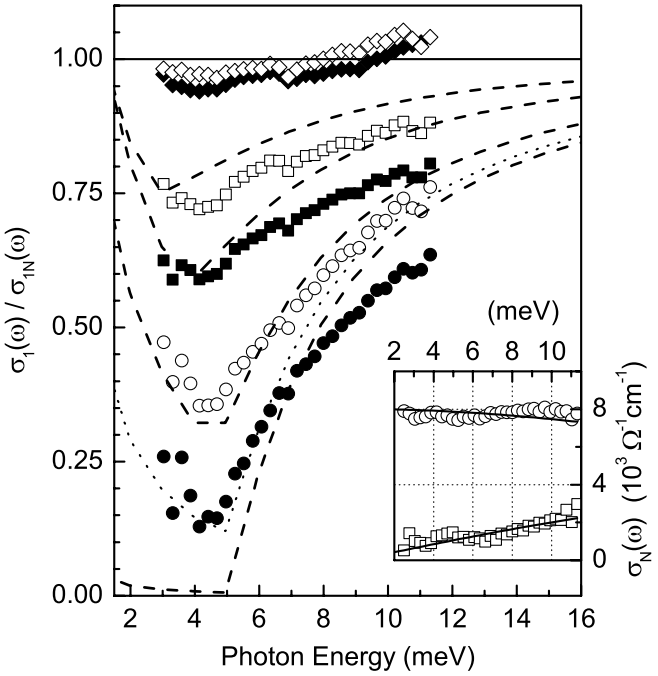

FIG. 2. Real part of conductivity $\sigma_1(\omega)$ for the 100 nm film normalized to its normal state value $\sigma_{1N}(40\ \mathrm{K})$ for $T = 6$ K (dots), 17.5 K (open circles), 24 K (solid squares), 27 K (open squares), 30 K (solid diamonds), and 50 K (open diamonds). Mattis-Bardeen calculations for $2\Delta_0 = 5$ meV, $T_C = 30$ K are shown (dashed and dotted lines, bottom to top) for 6, 12, 17.5, 24, and 27 K. Inset: real (circles) and imaginary (squares) part of normal state conductivity at 40 K, along with a Drude calculation (lines) explained in the text.

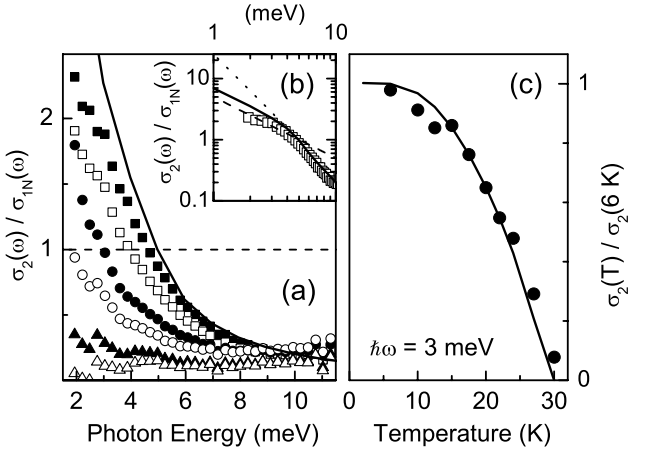

FIG. 3. (a) Imaginary part of conductivity $\sigma_2(\omega)$ normalized to the normal state value σ_{1N} at $T = 40$ K. Results are for $T = 6$ K (solid squares), 17.5 K (open squares), 24 K (dots), 27 K (open circles), 30 K (solid triangles), and 33 K (open triangles). Solid line: Mattis-Bardeen calculation for $T = 6$ K (parameters, see Fig. 2). (b) Data from (a) at $T = 6$ K (open squares) in a double log plot, compared to $\sigma_2(\omega) \sim \omega^{-1}$ (dashed line), $\sigma_2(\omega) \sim \omega^{-2}$ (dotted line), and the Mattis-Bardeen result at 6 K (solid line). (c) Normalized temperature dependence of $\sigma_2(3\ \mathrm{meV})$ (solid circles), compared to the Mattis-Bardeen result at this frequency (solid line).

are given in Fig. 3(a) [symbols]. In the superconducting state, $\sigma_2(\omega)$ shows the typical shape indicative of the supercurrent's high-frequency electromagnetic response, falling off strongly with photon energy and decreasing with temperature.

We now discuss the spectral shape and temperature dependence of the observed far-infrared conductivity. For comparison, calculations were performed using the theory of Mattis and Bardeen for an isotropic s-wave gap [24]. In view of the lower energy threshold of the observed absorption onset, an artificially small gap value of $2\Delta_0 = 5$ meV was chosen. The results of such calculations at different temperatures are shown in Fig. 2 (dashed lines) where the gap $\Delta(T)$ was assumed to follow the usual BCS temperature dependence. The calculated absorption sets in above $2\Delta_0$ and converges to the normal state conductivity at higher photon energies. In addition, a low-frequency Drude-like component due to thermally activated normal carriers gains weight with increasing temperature. We emphasize that the experimental data follow this overall trend in frequency and temperature dependence. A slower rise with photon energy is observed in the experiment, however, and some low-frequency residual conductivity remains at the lowest temperature which could also result from a slightly larger film temperature (dotted line, Fig. 2). Most strikingly, the value of the absorption onset is almost a factor of 2 smaller than even the value $2\Delta_0 = 3.5 k_B T_C \approx 9$ meV expected in a weak-coupling scenario.

The calculated imaginary part of the conductivity shown in Fig. 3(a) (solid line) for the lowest temperature of 6 K comes close to the experimentally observed frequency dependence. The shape of $\sigma_2(\omega)$ is illustrated in Fig. 3(b), where the experimental data (open squares) are compared to the London limit ω^{-1} (dashed line) and to ω^{-2} (dotted line). In our frequency range, the data transits from the low-frequency ω^{-1} behavior observed by Pronin *et al.* [20] into $\sigma_2(\omega) \sim \omega^{-2}$ for photon energies larger than $\hbar\omega \gtrsim 5$ meV. The full Mattis-Bardeen calculation [solid line, Fig. 3(b)] yields a faithful representation of this transition which is due to the onset of dissipative excitations across the gap.

The penetration depth λ can, in principle, be obtained from the optical conductivity at frequencies sufficiently below the gap, where $\lambda^{-2}(T) = \mu_0 \omega \sigma_2(\omega, T)$. Since our data sparsely overlaps with the ω^{-1} regime, a rough estimate of $\lambda(0) \approx 300$ nm can be obtained from the conductivity at the lowest available temperature and photon energy. More insight is obtained from the temperature dependence of σ_2, which is plotted in Figure 3(c) for 3 meV (dots). Within the experimental accuracy, satisfactory agreement is found with the Mattis-Bardeen calculation at the given frequency (solid line). The data thus indicate that despite the lowered gap size, the condensate that evokes this inductive σ_2 response follows the BCS temperature dependence quite well.

One particularly intriguing result of this study is the persistently small size of the conductivity gap as compared to the transition temperature. Here, we find a ratio of only $2\Delta_0/k_BT_C = 1.9$, which is far below the usual weak- or strong-coupling BCS values. Our experiment shows that the dramatic transmission changes observed in this spectral range [Fig. 1(b)] are ultimately linked to the emergence of this conductivity gap as in conventional metals [17]. The *identical* spectral position of such transmission changes for both samples investigated here, as well as that from a different study [19], points to a more robust nature of this observation.

We emphasize that this reduced ratio cannot be due to a sample inhomogeneity in which percolative paths through regions with increased gap would yield the transport T_C, whereas the bulk fraction of the sample would become superconducting at a much lower temperature linked to the smaller gap via the usual BCS ratio. This scenario is not possible since our optically measured imaginary part of the conductivity, which probes the complete volume of the film, shows directly that the major fraction of the condensate persists up to the large transport-derived T_C.

One likely explanation of the observed small gap can arise from the proposed two-gap scenario [14]. In that case, our observed conductivity gap corresponds to the smaller order parameter, whereas the larger one lies outside our optically accessible range. We observe that $\sigma_1(\omega)$ rises slower with photon energy than predicted by the isotropic calculations, which might support this contention. Anderson's theory of dirty-limit superconductors shows that the gap size for a single isotropic order parameter is not affected by nonmagnetic impurity scattering, but a two-gap state could nevertheless be averaged out to give the usual weak- or strong-coupling value [25,26]. However, the two-gap state should persist for predominantly *intraband* nonmagnetic scattering [27], e.g., for small-angle impurity scattering which lacks the momentum to scatter holes between the quasi-2D and 3D Fermi surfaces well separated in momentum space. Comprehensive theoretical calculations of the optical and other fundamental physical properties are imperative to achieve a full understanding of the low-energy excitations in MgB_2.

In summary, we have studied the far-infrared conductivity of thin MgB_2 films using terahertz time-domain spectroscopy in a broad spectral range. The complex conductivity exhibits the characteristic electrodynamic response of a dirty-limit metal in the normal state. An inductive response in the imaginary part appears below T_C due to the emergence of the superconducting condensate. A strong depletion of the real part of the conductivity corresponds to the opening of a low-energy superconducting gap, yet its energy threshold $2\Delta \approx 5$ meV is only half that expected in an isotropic, weak-coupling theory.

This work was supported by the U.S. Department of Energy, Office of Science, under Contracts No. DE-AC03-76SF00098 and No. DE-AC05-00OR22725. R. A. K. gratefully acknowledges financial support from the Deutsche Forschungsgemeinschaft.

[1] J. Nagamatsu *et al.,* Nature (London) **410**, 63 (2001).
[2] S. L. Budko *et al.,* Phys. Rev. Lett. **86**, 1877 (2001).
[3] D. G. Hinks, H. Claus, and J. D. Jorgensen, Nature (London) **411**, 457 (2001).
[4] F. Bouquet *et al.,* Phys. Rev. Lett. **87**, 047001 (2001).
[5] Ch. Wälti *et al.,* Phys. Rev. B **64**, 172515 (2001).
[6] X. K. Chen *et al.,* Phys. Rev. Lett. **87**, 157002 (2001).
[7] J. W. Quilty, S. Lee, A. Yamamoto, and S. Tajima, cond-mat/0107216.
[8] G. Rubio-Bollinger, H. Suderow, and S. Vieira, Phys. Rev. Lett. **86**, 5582 (2001).
[9] H. Schmidt *et al.,* Phys. Rev. B **63**, 220504(R) (2001).
[10] S. Tsuda *et al.,* Phys. Rev. Lett. **87**, 177006 (2001).
[11] F. Giubileo *et al.,* Phys. Rev. Lett. **87**, 177008 (2001); cond-mat/0105146, and references therein.
[12] P. Szabo *et al.,* Phys. Rev. Lett. **87**, 137005 (2001).
[13] J. Kortus *et al.,* Phys. Rev. Lett. **86**, 4656 (2001).
[14] A. Y. Liu, I. I. Mazin, and J. Kortus, Phys. Rev. Lett. **87**, 087005 (2001).
[15] D. Manske, C. Joas, I. Eremin, and K. H. Bennemann, cond-mat/0105507.
[16] A. S. Alexandrov, cond-mat/0104413.
[17] L. H. Palmer and M. Tinkham, Phys. Rev. **165**, 588 (1968).
[18] B. Gorschunov *et al.,* Eur. Phys. J. B **21**, 159 (2001).
[19] J. H. Jung *et al.,* cond-mat/0105180.
[20] A. V. Pronin, A. Pimenov, A. Loidl, and S. I. Krasnosvobodtsev, Phys. Rev. Lett. **87**, 097003 (2001).
[21] M. Paranthaman *et al.,* Appl. Phys. Lett. **78**, 3669 (2001).
[22] Such extremely thin films exhibit T_C's smaller than optimal, yet with quite sharp transitions $\Delta T_C \approx 1$ K, resulting most likely from a slightly depressed density of states at the Fermi level due to disorder.
[23] M. C. Nuss and J. Orenstein, in *Millimeter and Submillimeter Wave Spectroscopy of Solids,* edited by G. Grüner (Springer-Verlag, Berlin, 1998), and references therein.
[24] D. C. Mattis and J. Bardeen, Phys. Rev. **111**, 412 (1958).
[25] P. W. Anderson, J. Phys. Chem. Solids **11**, 26 (1959).
[26] We rule out magnetic impurities since (i) energy-dispersive x-ray analysis shows no detectable traces of such elements; (ii) expected strong variations of the spectral gap position with T_C remain unobserved (cf. Fig. 1).
[27] A. A. Golubov and I. I. Mazin, Phys. Rev. B **55**, 15 146 (1997).